2015

The role of free surfaces on the formation of prismatic dislocation loops

Lynn B. Munday
RDRL-CIH-C, U.S. Army Research Laboratory, Aberdeen Proving Ground, MD

Joshua C. Crone
RDRL-CIH-C, U.S. Army Research Laboratory, Aberdeen Proving Ground, MD

Jaroslaw Knap
RDRL-CIH-C, U.S. Army Research Laboratory, Aberdeen Proving Ground, MD

Available online at www.sciencedirect.com

ScienceDirect

Scripta Materialia 103 (2015) 65–68

Scripta MATERIALIA

www.elsevier.com/locate/scriptamat

The role of free surfaces on the formation of prismatic dislocation loops

Lynn B. Munday,* Joshua C. Crone and Jaroslaw Knap

RDRL-CIH-C, U.S. Army Research Laboratory, Aberdeen Proving Ground, MD 21005, USA

Received 27 January 2015; revised 3 March 2015; accepted 3 March 2015
Available online 28 March 2015

Prismatic punching is a process where voids grow through the nucleation and emission of prismatic dislocation loops (PDLs). In this work we employ dislocation dynamics to determine the effect of image stresses produced by the void's free surface on PDL formation in a face-centered cubic lattice. We find that image stresses cause PDL formation to fall into two distinct pressure regimes. In the low pressure regime, image stresses dominate dislocation cross-slip, reducing the PDL's size and formation rate.
Published by Elsevier Ltd. on behalf of Acta Materialia Inc.

Keywords: Dislocation dynamics; Void growth; Image stress; Cross-slip

During the initial stages of void growth, dislocations nucleated from the void's surface are assumed to punch out material from the void [1]. However, dislocations nucleated as glide loops with a Burgers vector in the plane of the loop cannot remove material. It is only after the conversion of the glide loop into a prismatic dislocation loop (PDL) with a Burgers vector normal to the loop that material removal through punching is possible [2]. The conversion from a nucleated dislocation into a PDL can occur through an interaction with dislocations on other glide planes or through multiple cross-slip events [3,4]. In both formation mechanisms, the PDL is assumed to form under the action of the stress concentrators arising from the far-field load's interaction with the void. In this letter we report a new limiting factor on PDL formation. We show that image stresses produced by the interaction of the dislocation with the void's free surface dominate PDL formation for pressures below 3.0 GPa and limit void growth.

Plastic void growth occurs during the ductile failure process where high-strain loading leads to void nucleation, growth, and coalescence into microcracks. After a nano-sized void is nucleated at a weak spot in the lattice, it grows plastically through dislocation related processes. The initial stages of void growth occurs through the nucleation of dislocations from the void's surface [3,5]. Dislocation nucleation remains active up to micron sized voids at which point the density of dislocations in the material becomes large enough to support continued plastic growth through dislocation multiplication [6]. At the early stages, submicron void growth becomes strongly dependent on the discrete volume changes due to the formation and emission of individual PDLs.

High strain rates and small void sizes, typical for atomistic simulations, reveal PDL formation via interaction of multiple nucleated dislocation loops on different glide planes [3]. In a stark contrast to the high-strain rate simulations, Ashby and Johnson [4] describe a fully 3D mechanism for PDL formation around a spherical particle as originating from a single incipient dislocation loop. In their model, the misfit particle induces a stress field equivalent to that of a void under far-field hydrostatic stress [7]. Under the action of this stress field, the incipient dislocation loop expands out from the particle, cross-slipping onto other glide planes once it becomes energetically favourable. After a sequence of four cross-slip events, a PDL is finally formed.

Ashby and Johnson's model was developed for PDL formation around a particle and therefore does not include the effect of the void's free surface on dislocation cross-slip. However, image forces arising from the dislocation's interaction with the free surface have been shown to be influential on cross-slip in previous atomistic and dislocation dynamics simulations [8,9]. In this work, we employ 3D dislocation dynamics to determine the effects of these image stresses on the mechanisms which allow an incipient dislocation loop nucleated from the surface of a void to evolve into a PDL. Our simulations are based on the dislocation dynamics formulation of van der Giessen and Needleman [10]. In this formulation, the stress fields due to dislocations in an infinite perfect crystal are combined with those obtained from a solution of an auxiliary boundary value problem with suitable traction boundary conditions. We utilize the Parallel Dislocation Simulator (ParaDiS) [11] for the former and a parallel finite element code for the latter [12,13].

* Corresponding author; e-mail: lynn.b.munday.civ@mail.mil

http://dx.doi.org/10.1016/j.scriptamat.2015.03.009
1359-6462/Published by Elsevier Ltd. on behalf of Acta Materialia Inc.

The material considered is a model face-centered cubic (fcc) crystal of aluminum with shear modulus $\mu = 27$ GPa, Poisson's ratio $\nu = 0.35$ and Burgers vector magnitude $|\mathbf{b}| = 2.86$ Å. A linear mobility function is employed to relate the force on the dislocation to its velocity through $f_i = B_i v_i$. Here, f is the dislocation force, B is the drag coefficient, v is the dislocation velocity and subscript i indicates the dislocation character, either edge or screw. We assume that drag coefficients in the linear mobility function satisfy $B_{screw}/B_{edge} = 2$. The above ratio has been determined by Olmsted et al. [14] from atomistic simulations. We emphasize that according to this mobility function, the same stress value will propel edge dislocations to move twice as fast as screw dislocations. Thus, screw oriented dislocations able to cross-slip will be preferred. Moreover, since only dislocations with a full Burgers vector are modeled, cross-slip of screw dislocations will occur once stresses become favourable. Finally, we emphasize that the local force on the dislocation includes Peach–Koehler forces from other dislocations and the far-field loading as well as the dislocation's self-energy by recourse to the line-tension model.

Our computational domain is a cube of edge length $l = 25{,}000\ |\mathbf{b}|$ containing a single void of radius $R_v = 100\ |\mathbf{b}|$ at the center. Tractions imposing a uniform stress field $\boldsymbol{\sigma}^\infty = p\mathbf{I}$, where $\mathbf{I}$ is the identity tensor and $p > 0$, are applied to the outer cube boundaries. It bears emphasis that pressure p is being defined as hydrostatic tension. Image tractions due to the dislocations are applied to the void surface. We discretize the computational domain with variable sized quadratic tetrahedral elements yielding a 2.5 $|\mathbf{b}|$ resolution in the vicinity of the void.

Dislocation nucleation is not examined in the present work and all dislocations are assumed to originate from an incipient dislocation structure. The nucleation of any incipient dislocation structure around the void is driven by the resolved shear stress on a glide plane defined as $\sigma_{bn} = \hat{\mathbf{n}} \cdot \boldsymbol{\sigma} \cdot \hat{\mathbf{b}}$, where $\boldsymbol{\sigma}, \hat{\mathbf{b}} = \mathbf{b}/|\mathbf{b}|$, $\hat{\mathbf{n}} = \mathbf{n}/|\mathbf{n}|$ are the stress, the unit Burgers vector and the unit normal of the glide plane, respectively. In Figure 1, we plot σ_{bn} in the region near the void for the two families of glide planes: (a) $\mathbf{n} = (1\,1\,1)$ and (b) $\mathbf{n} = (\bar{1}\,\bar{1}\,1)$ sharing the Burgers vector $\mathbf{b} = [\bar{1}\,1\,0]$. An ideal PDL with $\mathbf{b} = [\bar{1}\,1\,0]$ shown by the blue and red lines in Figure 1(c) is made up of a continuous dislocation loop gliding on these families of glide planes denoted by the dashed lines and numbered (*i*) through (*iv*). The Burgers vector $\mathbf{b} = [\bar{1}\,1\,0]$ of this PDL is oriented toward the reader. Under the action of $\boldsymbol{\sigma}^\infty$, the maximum of $\sigma_{bn} = \pm\frac{3}{4}p$ for each of the two glide planes is located at a distance of $R_v/\sqrt{2}$ from the center. In order to mimic the effect of dislocation nucleation in our simulations, an incipient dislocation configuration composed of a $[\bar{1}\,1\,0](1\,1\,1)$-type dislocation glide loop with radius $R_L = 25\ |\mathbf{b}|$ is placed on the void surface at the position of the maximum resolved shear stress, as indicated in Figure 1(c). We emphasize that this incipient dislocation loop is not always stable as it is drawn into the void if $p \leqslant 1.4$ GPa.

We start by assessing the sequence of events assumed by Ashby and Johnson's classical model for PDL formation. In order to account for free surfaces in our simulations, dislocations intersecting the surface are terminated with the end on the surface constrained to move along the surface. Moreover, we approximate free surface effects on the dislocation self energy by removing line-tension forces at the surface. We connect dislocation surface nodes via so-called virtual dislocations to the center of the void as to maintain a zero net Burgers vector for the surface terminated dislocations [15]. We point out that the above

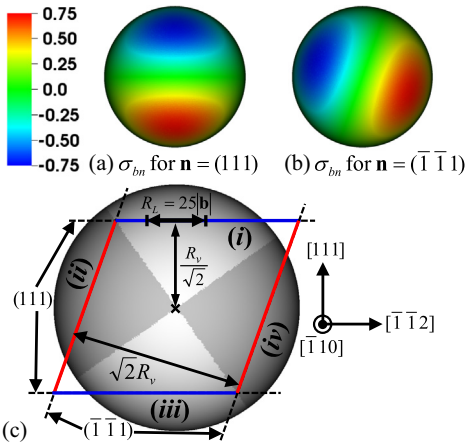

Figure 1. Glide stress due to the far-field load near the void surface for $\mathbf{b} = [\bar{1}\,1\,0]$ and glide plane normals (a) $\mathbf{n} = (1\,1\,1)$ or (b) $\mathbf{n} = (\bar{1}\,\bar{1}\,1)$. The colourbar shows the normalized stress, σ_{bn}/p. (c) Void surface coloured by the glide plane maximizing σ_{bn}. The light grey quadrant indicates the region where $|\sigma_{b\mathbf{n}=(1\,1\,1)}| > |\sigma_{b\mathbf{n}=(\bar{1}\,\bar{1}\,1)}|$ and dark grey indicates the opposite. Light grey quadrants favour growth of $[\bar{1}\,1\,0](1\,1\,1)$ type dislocations shown in blue and dark grey quadrants favour growth of $[\bar{1}\,1\,0](\bar{1}\,\bar{1}\,1)$ type dislocations shown in red. The incipient $[\bar{1}\,1\,0](1\,1\,1)$ dislocation loop is dimensioned and labeled R_L. The red and blue lines indicate the ideal PDL that would be generated from the incipient dislocation and passes through points maximizing σ_{bn}. Each glide plane of the PDL is labeled (*i*–*iv*). (For interpretation of the references to colour in this figure legend, the reader is referred to the web version of this article.)

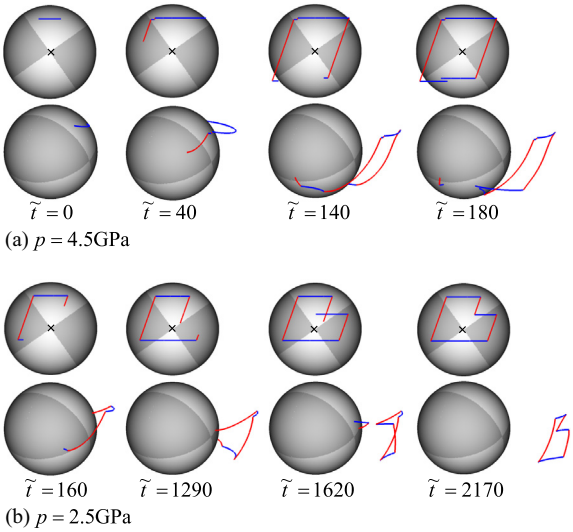

Figure 2. Evolution of an incipient dislocation loop into a PDL for (a) $p = 4.5$ GPa and (b) $p = 2.5$ GPa. Two views of the PDL are shown at each time step labeled by $\tilde{t}$ with units GPa^{-1}. The top view showing the contour of the PDL uses the coordinate system in Figure 1. The lower view shows the profile of the PDL peeling off in the $\mathbf{b} = [\bar{1}\,1\,0]$ direction. Dislocation and void quadrant colouring are described in Figure 1(c).

modifications are in addition to the image stresses being computed by the corrective boundary value problem.

In Figure 2(a) we plot the evolution of the incipient dislocation loop for $p = 4.5$ GPa. Two views are given at each timestamp labeled by the normalized time, $\tilde{t} = t/B_{screw}$, where t is simulation time. The upper view shows the contour of the PDL while the lower view provides a profile of the PDL peeling off the void. In the following description of events, the glide planes will be referred to by (*i–iv*) as described in Figure 1(c). The incipient dislocation loop is shown at $\tilde{t} = 0$. In the sequence of snapshots which follows, the incipient dislocation loop undergoes cross-slip near light and dark grey boundaries, as expected on the basis of the far-field loading. In the final snapshot at $\tilde{t} = 180$ the two sides of the dislocation loop moving on glide plane (*iii*) pass one another forming a full PDL but fail to annihilate. Afterwards, the two ends of the PDL continue to circle the void emitting additional PDLs, which remain linked together. The above sequence of events is in good agreement with the model of Ashby and Johnson. It is important to point out that such a sequence has been reported previously by Geslin et al. [16] for a misfit particle in a simple cubic crystal. One minor difference, due solely to the underlying fcc crystallography, is that cross-slip from (*ii*) to (*iii*) shown for $\tilde{t} = 140$ occurs on a bulk portion of the dislocation line as opposed to cross-slip of the surface dislocation.

The next sequence of snapshots in Figure 2(b) represents the evolution of a PDL at $p = 2.5$ GPa. As before, this sequence originates from the same incipient dislocation structure shown for $\tilde{t} = 0$ in Figure 2(a). However, its progression towards a PDL is dramatically different. The major difference between this sequence and that for $p = 4.5$ GPa is the location of cross-slip events. At $\tilde{t} = 160$ cross-slip from (*i*) to (*iv*) and (*ii*) to (*iii*) occurs prematurely based on the far-field loading, i.e. before the dislocation reaches the dark grey quadrant. This cross-slip event causes the leading edges of the dislocations at $\tilde{t} = 1290$, shown gliding across the void surface on (*iii*) and (*iv*), to move into regions where σ_{bn} in Figure 1(a and b) is nearly zero. After crossing into these low stress regions, the dislocation on (*iii*) undergoes several surface cross-slip events to produce the full PDL shown at $\tilde{t} = 1620$ where the two sides of the dislocation loop annihilate one another. After the PDL is formed, a small section of it is cut-off at $\tilde{t} = 1620$ and pulled back into the void, resulting in the PDL contour shown at $\tilde{t} = 2170$. All cross-slip events during the formation of this PDL occur on the void surface.

Based on results in Figure 2, it is evident that there exist two distinct evolution paths for the formation of a PDL. Furthermore, the selection of any of the two paths is a function of the applied pressure, p. At the higher pressure of $p = 4.5$ GPa, PDL formation is controlled by the applied load as cross-slip occurs at locations predicted by the model of Ashby and Johnson. In contrast, at the lower pressure of $p = 2.5$ GPa, cross-slip does not occur at locations predicted by the model. We attribute the difference primarily to image stresses induced by the void surface.

The image stress is highest near the void surface where it attempts to orient the surface piercing dislocation into its lowest energy configuration. This configuration is a balance between minimizing the dislocation's length and edge component [17]. For the void geometry, the dislocation with the lowest energy would be purely screw and located at the center of the void surface marked by a black "×" in the figures. For the case of the incipient dislocation loop, image stresses push the surface dislocation toward cross-slip onto $(\bar{1}\,\bar{1}\,1)$. However, the resolved shear stresses from the far-field load push the dislocation to continue gliding on $(1\,1\,1)$. Cross-slip due to the far-field load is only favoured when the resolved shear stress on the secondary plane becomes greater than that on the primary plane, i.e. the interface between the light and dark grey regions in the figures. Therefore, the dominance of either the image stress or far-field loading determines the location of cross-slip and in effect the contour of the PDL.

We now present a series of simulation results in Figure 3(a and b) aimed at determining the pressure range of each regime. We plot the final PDL contours over a range of $p = 1.5$–4.5 GPa in 0.5 GPa increments. The contours in the image stress mediated regime ($p = 1.5$–3.0 GPa) are shown in Figure 3(a). All of the contours dominated by the image stress show at least one premature cross-slip event at a location not favoured by the far-field load. Premature cross-slip causes the dislocation to trace out a path where the resolved shear stresses are reduced when compared to those experienced by the ideal PDL contour indicated by the dashed black line. This reduction in resolved shear stress yields partially formed PDLs for $p = 1.5$ and 2.0 GPa with final configurations similar to those in Figure 2(b) at $\tilde{t} = 160$. The pressure dominated regime occurs for $p \geq 3.5$ GPa. We remark that the PDLs generated in the high pressure regime are larger and remove more material from the void than those formed in the image stress dominated regime. The contour formed at $p = 3.0$ GPa shows signs of both regimes where cross-slip on one arm of the PDL is dominated by image stress while the other arm follows a route closer to that predicted by the pressure dominated regime.

In order to elucidate further the role of the image stress, we perform simulations of PDL formation in the vicinity of a misfit particle. The misfit particle is formed by filling in the void with the surrounding material. A uniform dilatation is applied to the misfit particle as to produce the same σ_{bn} as for the case of the void under p. Interior to the misfit

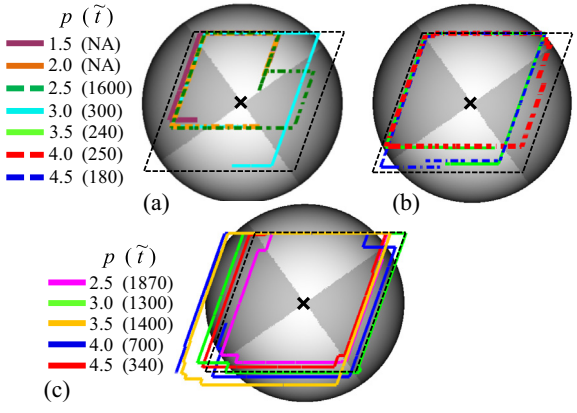

Figure 3. PDL contours for (a) image stress dominated cross-slip, (b) pressure dominated cross-slip and (c) misfit particle. The dashed black line indicates the ideal PDL. PDL colours are labeled in the legend by the far-field load, p, with units GPa. The normalized time, $\tilde{t}$, for the formation of the PDL is given in parentheses with units GPa^{-1}. (For interpretation of the references to colour in this figure legend, the reader is referred to the web version of this article.)

particle, the stress field is purely hydrostatic with $\sigma_{bn} = 0$. The misfit particle does not contain free surfaces and therefore dislocations are not terminated at the interface and no image stresses are produced. Under these conditions two PDLs are formed. The first one extends in the interior of the particle, while the second one in the opposite direction. The PDL contours of the second PDL as a function of p are plotted in Figure 3(c). In contrast with the results for the void, no dependence on p is observed as the PDLs follow closely the sequence of events of Ashby and Johnson.

Our results demonstrate the importance of image stresses on PDL formation from a void. The influence of image stresses is most pronounced in the low pressure regime (c.f. Fig. 3(a)). Under these conditions, the image stress controls dislocation cross-slip and is a critical component of deformation mechanisms. For simple planar geometries, the elastic interaction between a dislocation and a free surface causes simply rotation of the dislocation as to minimize the energy associated with its character and length [17]. However, surfaces endowed with more complex geometry are likely to play an even more significant role, not only in the orientation of surface dislocations, but also in their overall motion by affecting cross-slip. Here, the spherical geometry of the void was solely responsible for initiating early cross-slip on the void surface. Similar geometry mediated cross-slip has been observed in both atomistic and dislocation dynamics simulations of micropillar deformation [8]. In this case, cross-slip led to a dislocation self-multiplication mechanism which explained the experimentally observed increase in plasticity of base-centered cubic micropillars [8,9]. However, the atomistic simulations also showed partial dislocations in fcc micropillars suppressing this geometry dependent cross-slip [8].

Image stresses are shown to be less influential on cross-slip for the high pressure regime. Still, it is unclear how easily this regime is accessible in practice. Atomistic simulations of dislocation emission from voids of size $R_v = 15$–$40\ |\mathbf{b}|$ indicate dislocation nucleation when $\sigma_{bn} \approx 0.1\mu$, which corresponds to $p \approx \frac{4}{30}\mu$ [18,5]. For aluminum considered here, dislocation nucleation would then be expected at $p \approx 3.6$ GPa, well within the high pressure regime. However, results of atomistic studies suggest that the dislocation nucleation threshold is a function of both the strain rate and void size [18,5,19]. Analytical models extrapolating from the atomistic data to larger void sizes ($R_v > 40|\mathbf{b}|$) and slower strain rates ($\dot{\epsilon} = 10^6$/s) find the dislocation nucleation threshold dropping to $p \approx 2.5$ GPa [1,19]. At pressures this low, PDL formation would be dominated by image stress.

We have provided a new perspective on the role of free surfaces on void growth via PDL formation. The image stress, due to the presence of the free surface, causes PDL formation to occur through a different mechanism in two separate pressure regimes. In the high pressure regime, the far-field stress dominates cross-slip and PDL formation. Ashby and Johnson's [4] model for PDL formation is found applicable to both a void in this high pressure regime and a misfit particle. In the low pressure regime, image stress controls cross-slip causing PDL formation to deviate significantly from the sequence of events described by Ashby and Johnson [4]. This deviation leads to the formation of smaller PDLs. In contrast, PDLs formed in the absence of free surfaces around a misfit particle do not exhibit the same pressure dependence. Therefore, free surfaces play a vital role in the evolution of dislocations near a void.

Support of the U.S. Army Research Laboratory's Enterprise for Multiscale Research of Materials is gratefully acknowledged. Computing support was provided by the DoD Supercomputing Resource Center located at the U.S. Army Research Laboratory.

[1] V. Lubarda, M. Schneider, D. Kalantar, B. Remington, M. Meyers, Acta Mater. 52 (2004) 1397.
[2] V. Bulatov, W. Wolfer, M. Kumar, Scr. Mater. 63 (2010) 144.
[3] T. Tsuru, Y. Shibutani, J. Phys. D: Appl. Phys. 40 (2007) 2183.
[4] M. Ashby, L. Johnson, Philos. Mag. 20 (1969) 1009.
[5] R. Rudd, Philos. Mag. 89 (2009) 3133.
[6] H.-J. Chang, J. Segurado, J. LLorca, Scr. Mater. 95 (2015) 11.
[7] J. Eshelby, Proc. R. Soc. Lond., Ser. A 241 (1957) 376.
[8] C. Weinberger, W. Cai, Proc. Natl. Acad. Sci. 105 (2008) 14304.
[9] J. Greer, C. Weinberger, W. Cai, Mater. Sci. Eng. A 493 (2008) 21.
[10] E. Van der Giessen, A. Needleman, Modell. Simul. Mater. Sci. Eng. 3 (1995) 689.
[11] A. Arsenlis, W. Cai, M. Tang, M. Rhee, T. Oppelstrup, G. Hommes, T. Pierce, V. Bulatov, Modell. Simul. Mater. Sci. Eng. 15 (2007) 553.
[12] K. Leiter, J. Crone, J. Knap, J. Comput. Sci. 4 (2013) 401.
[13] J. Crone, P. Chung, K. Leiter, J. Knap, S. Aubry, G. Hommes, A. Arsenlis, Modell. Simul. Mater. Sci. Eng. 22 (2014) 035014.
[14] D. Olmsted, L. Hector Jr, W. Curtin, R. Clifton, Modell. Simul. Mater. Sci. Eng. 13 (2005) 371.
[15] D. Weygand, L. Friedman, E. Van der Giessen, A. Needleman, Modell. Simul. Mater. Sci. Eng. 10 (2002) 437.
[16] P. Geslin, B. Appolaire, A. Finel, Acta Mater. 71 (2014) 80.
[17] C. Weinberger, S. Aubry, S.-W. Lee, W. Nix, W. Cai, Modell. Simul. Mater. Sci. Eng. 17 (2009) 075007.
[18] E. Seppälä, J. Belak, R. Rudd, Phys. Rev. B 69 (2004) 134101.
[19] L. Nguyen, D. Warner, Phys. Rev. Lett. 108 (2012) 035501.